RSC Advances

PAPER

View Article Online
View Journal | View Issue

Cite this: *RSC Adv.*, 2016, **6**, 104010

Large size nitrogen-doped graphene-coated graphite for high performance lithium-ion battery anode†

Xiaoxu Liu,*[ab] Erjia Liu,[c] Dongliang Chao,[c] Liang Chen,[a] Shikun Liu,[a] Jing Wang,[a] Yao Li,*[a] Jiupeng Zhao,[a] Yong-Mook Kang*[d] and Zexiang Shen[c]

Received 18th September 2016
Accepted 21st October 2016

DOI: 10.1039/c6ra23228k

www.rsc.org/advances

The reversible capacity of commercial graphite anodes for lithium-ion batteries (LIBs) is in the range of 340–360 mA h g^{-1}, which is lower than the theoretical value (372 mA h g^{-1}). Pure graphene anodes with high reversible capacity (>372 mA h g^{-1}) are still not used for industrial production due to their high discharge-voltage plateau, low initial coulombic efficiency, low tap density, *etc.* Herein, we synthesized new carbon anodes using large-size nitrogen-doped graphene-coated commercial graphite anodes (named LGAs) in which the commercial graphite was wrapped by a number (<5) of nitrogen-doped graphene (LNG) layers. The electrochemical performance of the LGAs was similar to that of commercial graphite, and the high tap density, low discharge potential, and high initial coulombic efficiency of graphite were maintained. However, the LGAs with 1 wt% of LNG were able to achieve a reversible capacity of about 390 mA h g^{-1}, which surpassed the theoretical value of graphite. Meanwhile, the LGAs delivered a reversible capacity of about 164 mA h g^{-1} at the rate of 5C, which was more than two times higher than that of the pure commercial graphite anodes. The production cost could be kept low only at a very low weight percentage of graphene (1 wt%) in LGA, enabling the large-scale commercial application of graphene in LIBs. Such a simple and scalable method may also be applied to other anode systems, boosting their energy and power densities.

Introduction

Concerns over the exhaustion of fossil fuels coupled with the associated serious environmental pollution has motivated researchers to focus their attention on the development of clean energies,[1] such as solar, wind, and geothermal energy. These clean energies need to be efficiently stored for various applications, including but not limited to electronic devices, hybrid and electric vehicles, and communication equipment. Thus, the development of energy-storage devices with high energy and power densities is desperately needed. Lithium-ion batteries (LIBs) are one of the most promising candidates for clean energy storage because of their high energy density and long cycling life.[2] However, the energy storage capacity of current LIBs needs to be enhanced by innovating new electrode materials. Graphite used as an anode material of LIBs exhibits a lot of advantages regarding energy storage, such as its abundant resources, low cost, lack of environmental pollution, relatively large storage capacity, and good stability.[3] However, graphite materials are confined to a theoretical capacity of about 372 mA h g^{-1}, which has limited their application in large-scale energy storage. Hence, other anode materials, such as silicon,[4–9] germanium,[10] stannum,[11,12] *etc.*, have been greatly pursued for LIBs because of their low discharge potential, high theoretical capacity, and low cost. However, these anode materials suffer from severe capacity fading arising from the significant volume expansion that occurs during Li uptake and release processes. Various carbon-based materials, such as carbon nanotubes,[13,14] carbon fibers,[15,16] hard carbon,[17] and soft carbon,[18] have also been investigated in detail for the development of new carbonaceous anode materials with higher specific capacities than graphite. However, due to their low initial coulombic efficiency and high discharge-voltage plateau *etc.*, these carbon-based anode materials are still not suitable for the large-scale industrial production of LIBs.

Recently, graphene has attracted great research interest for its outstanding performance in electrochemical energy storage.[19–22] It has been reported that graphene-based anode materials have demonstrated great improvements, in particular regarding capacity and rate performance.[23–26] The capacity

[a]*Harbin Institute of Technology, Harbin, 150001, Heilongjiang, China. E-mail: liu88062321@126.com; liyao@hit.edu.cn*

[b]*Key Laboratory for Photonic and Electric Bandgap Materials, Ministry of Education, Heilongjiang University of Science and Technology, Harbin, Heilongjiang, China*

[c]*Nanyang Technological University, 50 Nanyang Avenue, 637371, Singapore*

[d]*Department of Energy and Materials Engineering, Dongguk University-Seoul, Seoul, Republic of Korea. E-mail: dake1234@dongguk.edu*

† Electronic supplementary information (ESI) available. See DOI: 10.1039/c6ra23228k

increase was attributed to the large surface areas, high conductivity, chemical stability, and extra space for Li-ion storage of graphene sheets. However, graphene-based electrodes for LIBs possess poor reversible capacity and cycle life due to their structural limits, such as the re-stacking of graphene sheets. Thus, pure graphene anodes for LIBs face several major challenges: first, reduced graphene usually possesses a very high specific surface area and very low tap density, which greatly decreases the initial volumetric capacity. Second, the preparation of graphene usually requires complicated processes and is costly. The number of graphene sheets is also difficult to control. Third, graphene-based anodes for LIBs have a high discharge-voltage plateau.[27] If a full cell is assembled using a graphene anode and a commercial cathode material, it would greatly decrease the outside potential and energy density of LIBs. Most importantly, the initial coulombic efficiency of graphene anodes is usually low[24] due to the formation of a solid–electrolyte interphase (SEI) layer, which consumes many of the Li ions supplied by the cathode. Currently, pure graphene as an anode material is still not used in the industrial production of LIBs.

In order to overcome the limitations in the application of graphene for LIBs, here, we report on composites of graphite after the incorporation of a few layers of large-size nitrogen-doped graphene (LNG) synthesized by the modified Hummers method. The composite comprising LNG and graphite was designated as LGA, and it was able to deliver a reversible capacity of 390 mA h g^{-1}, which is beyond the theoretical capacity of graphite (*i.e.*, 372 mA h g^{-1}). Compared with commercially available graphite, not only were the energy and power density of the LGA composite significantly improved, but also the high tap density, low discharge potential, and high initial efficiency of the original graphite were maintained as well. Because of the small amounts of graphene (1–3 wt%) in the composite, the production cost could be kept low compared to pure graphene anodes for LIBs. The easy scale-up of the modified Hummers method[28] also fulfills the conditions for large-scale applications of graphene.

Experimental

Preparation of large-size graphene oxide

Large-size graphene oxide (LGO) was prepared according to our reported method.[29] A small amount of expandable graphite was sealed in a glass vial. The vial was then heated in a commercial microwave oven for ~15 seconds under an ambient atmosphere to form worm-like graphite (WG). The LGO was prepared from WG according to the modified Hummers method. Next, 3 g of WG was added to concentrated sulfuric acid (400 ml) at 0 °C. Then, 6 g of $KMnO_4$ was added slowly until dissolved. The reaction was kept at 35 °C for 2 h. Next, the mixture was added to 400 ml deionized (DI) water and heated to 90 °C for 1 h. (Note: this solution is very corrosive. It reacts violently with organic material, and it must be treated with extreme caution.) The sediment was decanted, and the remaining solution was then centrifugated, washed with a total of 500 ml of 5% HCl solution three times, and then washed with DI water 10 times. Finally, the solution was centrifugated again and washed with DI water about 10 times to get the LGO solution (2 mg ml^{-1} aqueous dispersion).

Synthesis of large-size nitrogen-doped graphene-coated graphite anode

First, the colloidal LGO was dispersed in DI water at a concentration of 2 mg ml^{-1}, and a 60 min ultrasound treatment was performed to obtain a stable brown dispersion. Then, the LGO aqueous solution was added to commercial graphite powders with gentle stirring at room temperature. Then, the water solvents were evaporated by freeze-drying, and the powder color did not differ from that of the original graphite. Last, this LGO was transformed into N-doped reduced graphene under a hydrazine monohydrate vapor treatment at 120 °C,[30] and then a black LGA composite material was obtained.

Results and discussion

The synthesis process of the LGA composite material is schematically illustrated in Fig. 1 large-size graphene oxide (LGO) was prepared according to the modified Hummers method previously reported by us,[29] which has been considered the most popular approach to potentially scale-up the synthesis of graphene. To achieve a homogenous few-layer graphene coating on the surfaces of graphite, a LGO aqueous solution was dropwisely added to commercially available graphite powders under continuous stirring at room temperature (~22 °C). The LGO sheets were dispersed in the mixture, and they wrapped the surfaces of graphite particles through van der Waals interactions. Meanwhile, the water solvent was evaporated by freeze-drying, and the coated composite showed a color similar to that of the original graphite. In order to increase the conductivity, the LGO sheets were transformed into LNG sheets *via* a hydrazine monohydrate vapor treatment,[30] and then black

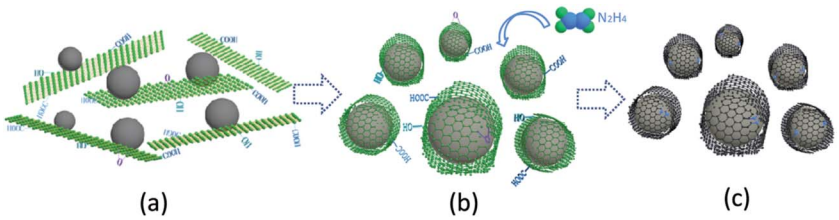

Fig. 1 Illustration of LGA synthesis process: (a) solution containing graphite and LGO, (b) graphite wrapped by LGO, and (c) LGA.

LGA composites were formed. In this process, LGO was reduced to conductive graphene, and nitrogen was introduced.

The LGO sheets used to wrap the graphite particles were obtained by repeated centrifugation of a LGO aqueous solution. The solution was centrifuged firstly at the speed of 3000 RPM to remove the unwanted large particles and then at the higher speed of 10 000 RPM to remove liquid supernatant containing very small GO sheets. The optimized centrifugation conditions to obtain large-sized few-layer graphene were obtained. Fig. 2a displays a typical optical micrograph of the graphene sheets with lateral sizes ranging from a few to several tens of micrometers. Fig. 2b shows an atomic force microscopy (AFM) image of a selected graphene sheet. The video that can be found in the ESI† shows that a large number of thin-layered, large-area graphene sheets were uniformly dispersed all over the Si substrate. Fig. 2c shows the statistical measurement results of the AFM thickness of 80 randomly selected sheets, ranging from 1 to 10 nm. Fig. 2d shows typical Raman spectra of LGO and LNG. Stronger D and G bands are observed at about 1350 and 1580 cm^{-1}. The I_D/I_G intensity ratio of LNG is obviously lower than that of LGO, suggesting that some oxygen-containing functional groups were removed during the reduction process. On the other hand, the 2D bands observed at about 2700 cm^{-1} indicate that both LGO and LNG sheets still possess good graphitic structures.

The morphology and microstructure of the LGA and original graphite were examined based on scanning electron microscopy (SEM) measurements. Fig. 3a–c show the SEM micrographs of the original synthetic graphite and LGA containing 1 and 3 wt% of LNG, respectively. It can be seen that the surfaces of the original graphite particles have clear boundaries and are apparently smooth (Fig. 3a). In contrast, the graphite particles were tightly encapsulated by LNG layers in the case of the LGA composites. The presence of crumpled and rough textures at the surfaces of LGAs is associated with the flexible and corrugated

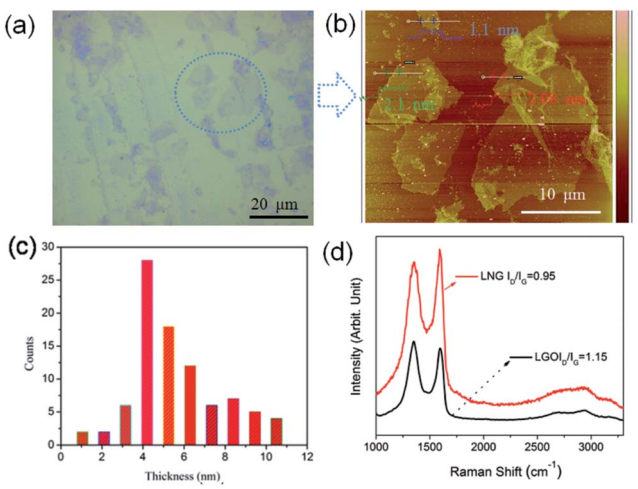

Fig. 2 (a) Optical micrograph of graphene platelets. (b) AFM image of selected graphene sheet. (c) Statistical measurement results of graphene thickness for 80 randomly selected sheets, where thickness ranges from 1 to 10 nm, and (d) Raman spectra (excited by 532 nm laser) of LGO and LNG.

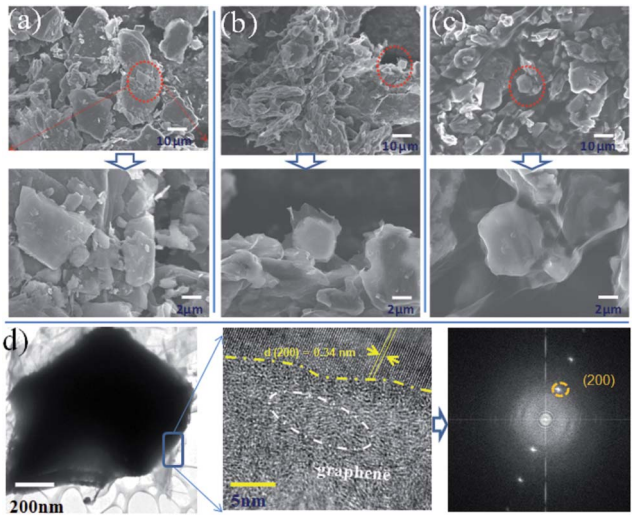

Fig. 3 SEM images of (a) pure graphite and (b, c) LGAs with 1 and 3 wt% LNG, respectively. (d) TEM images of LGA with 1% LNG.

nature of graphene sheets. Notably, individual LNG layers exposed around the surfaces of graphite particles can be identified in the LGA with 1 wt% of LNG (Fig. 3b). The surfaces of the graphite particles are nicely covered by the transparent graphene sheets and the ripples of the graphene layers are evident in Fig. 3c. The LNG sheets are favorable for the construction of 3D networks *via* crosslinking in the LGA containing 3 wt% of LNG. However, in the case of 5 wt% of LNG in the LGA composite, the uniform graphite particles are dispersed in the graphene sheets, which are formed by serious NG aggregation and loss of transparency (see Fig. S1†). Obviously, the SEM images of the LGA reveal that graphite is tightly enwrapped by graphene sheets and interconnected by the graphene networks. Therefore, such a unique geometric confinement of electrochemically active materials within the graphene matrix can effectively suppress the spalling of graphite during the charge–discharge processes and enhance the electrode stability against cyclic Li-storage processes (see below). To confirm LNG formation in the LGA composite, X-ray photoelectron spectroscopic (XPS) measurements were carried out. The XPS spectrum obtained exhibits C 1s, N 1s, and O 1s peaks at about 284, 400, and 533 eV, respectively, indicating the successful incorporation of nitrogen into graphene. The inset of Fig. S2a† shows the N 1s peak resolved into two components centered at about 399.7 and 400.8 eV that are assigned to pyridinic and pyrrolic nitrogen, respectively.[30] These findings are consistent with theoretical predictions and experimental observations from other researchers.[31,32] The X-ray diffraction patterns of pure graphite and the LGA with 1 wt% LNG are shown in Fig. S3,† in which both samples show similar (002) peaks in terms of peak position and symmetry, indicating that the general structural characteristics of the pure graphite are maintained in the LGA composite. In their Raman spectra (Fig. S4†), the pristine graphite exhibits a distinct G-band and a weak D-band with a correspondingly low I_D/I_G ratio, a typical feature of highly crystallized graphite. On the contrary, the I_D/I_G ratio of the LGA

becomes stronger with increasing LNG content, which confirms the formation of the LNG coating on the graphite surfaces. From the transmission electron microscopy (TEM) images of the LGA (see Fig. 3d), it can be seen that the micro-size graphite particles were tightly wrapped in giant N-doped graphene layers with the dents surrounding the graphite particles, which was in agreement with the SEM results. The high-resolution TEM image further reveals that the graphite particles were tightly anchored on the graphene sheets. The lattice fringe of the graphite with a space of 3.4 Å agrees well with the *d*-space of the (200) plane of the graphite. Besides, it is clearly observed that the multi-layered graphene on the boundary of graphite particles has a bent crystal lattice, which demonstrates the deeply LNG-encapsulated structure. The fast Fourier transform pattern further demonstrates that graphite and graphene simultaneously exist in the LGA composite.

In order to better understand the performance improvement, all samples including pure synthetic graphite and LGAs were cycled at the rates of 0.1C (*i.e.*, current density of 37.2 mAg^{-1}), 0.3C, 1C, 3C, 5C, and then reduced back to 0.1C (see Fig. 4a). At the rate of 0.1C, the LGAs with 1 wt% LNG loading provide reversible capacities. These values are higher than those reported for commercially available or synthetic graphite materials with various coatings.[33–39] Surprisingly, these values are even in excess of the theoretical value of 372 mA h g^{-1} for graphite. Moreover, no degradation in repeatability was observed for LGAs with different graphene content, as they could deliver higher than their original capacity if the rate was reduced back to 0.1C after successive cycling at various rates. Therefore, this repeatability is better than that of the original graphite. This improvement agrees with a previous report by Lain-Jong Li *et al.*[40] claiming that graphene-coated $LiFePO_4$ showed dramatically improved cathode performance. On the other hand, Fig. 4b shows the initial galvanostatic charge and discharge curves of the LGA and synthetic graphite anodes at the rate of 0.1C. It can be seen that the two samples have a similar low-voltage plateau and additional plateaus at 0.7 V, which generally correspond to the formation of an SEI film.[34] This result is consistent with cyclic voltammetry tests that show two peaks at 0.7 and 0.17 V in the anodic branch in the first cycles (see Fig. 4d). Meanwhile, the LGAs exhibited an initial coulombic efficiency of 87%, which makes their industrial application possible. Besides, LGA possess lightly higher discharge voltage plateau than pure graphite, which is benefited to inhibit the growth of lithium dendrites and improve battery safety. This can attribute to high voltage plateau of LNG (see Fig. S5†). Clearly, the treatment with LNG did not expand the irreversible capacity of graphite because of reversible redox reactions between the Li^+ ions and the LNG coating layer. The Nyquist impedance plots of the LGA and pure graphite anodes were also established and showed small loops and line parts (see Fig. 4c). In addition, the impedances of both the contact and the charge-transfer resistances of the LGA are lower than those of pure graphite. Meanwhile, with increasing LNG content, the impedances of the LGA gradually decrease (see Fig. S6†). These results indicate that the LGAs possess high reversible capacities and initial coulombic efficiencies. This can be attributed to the fact that the LNG coating layers not only have high reversible capacity but also provide a conductive network with excellent conductivity for electronic transport, which were proved four-point probe method (see Fig. S7 and S8†).

The electrochemical performance of the LGAs with 1, 3, and 5 wt% of LNG is further shown in Fig. 5. The discharge capacity performance of the graphite anode without LNG is also shown for comparison. As expected, on increasing the discharge rate, the capacity of pure graphite fades very quickly as the rate exceeds 1C. However, the LGAs with different LNG contents can

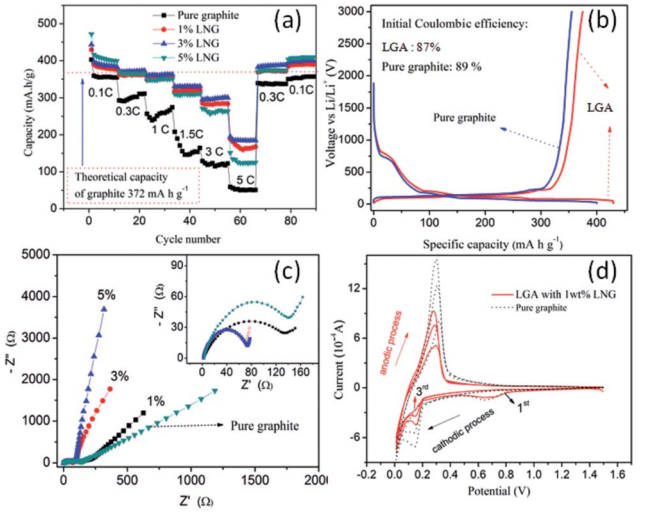

Fig. 4 (a) Rate capability of pure graphite and LGA anode with 1, 3, and 5 wt% (b) charge and discharge curves of LGA anode with 0 and 1% at 0.1C, (c) Nyquist plot of pure graphite and LGA with 1, 3, 5 wt% LNG, showing imaginary part *versus* real part, and (d) CV curves of the 1st, 2nd, and 3rd cycles of LGA composite with 1 wt% LNG and pure graphite.

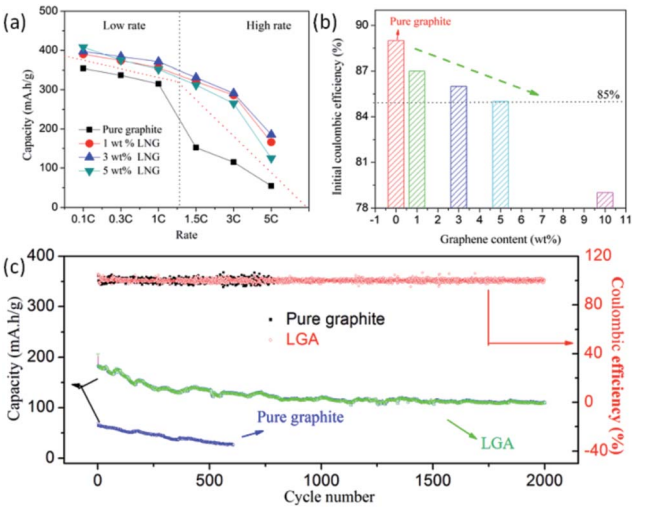

Fig. 5 (a) Discharge rate capability of LGA with 0, 1, 3, and 5% LNG, (b) initial coulombic efficiency of LGA with 0, 1, 3, and 5% LNG, and (c) lithiation/delithiation capacity and coulombic efficiency of LGA electrode cycled at rate of 5C for 2000 cycles.

deliver >12% higher capacity at lower rates of 0.1–1C. Moreover, the composite anode material LGA with 1 wt% of LNG can deliver a capacity of ~164 mA h g^{-1} at the high discharge rate of 5C, which is ~200% better than the 54 mA h g^{-1} obtained from pure graphite. Compared with pure graphite and other surface modified graphite (see Table S1†), the rate performance is substantially improved, particularly at high discharging rates. Besides, the initial coulombic efficiency of the LGA decreased as the LNG loading increased. However, all LGA samples showed coulombic efficiencies of more than 85% (Fig. 5b), and this result is accepted in practical applications.

To obtain long-cycling results within a reasonable testing period, faster charge and discharge tests with deep cycling (3–0.01 V) were carried out. Fig. 5c shows that at the high rate of 5C, the capacity of the LGA electrode is more than 100 mA h g^{-1} after 2000 cycles, thus indicating its superior and stable cycling performance. However, the pure graphite anode failed after 600 cycles. High coulombic efficiency is required for practical applications of the electrodes. For our LGA composite, the average coulombic efficiency from the second to the 2000th cycle is more than 98%, largely due to the formation of a stable SEI layer on the composite electrode.

From an industrial applications perspective, full cell performances are important for a new type carbonaceous anode. Herein, we used the commercial $LiCoO_2$ material as the cathode to be coupled with our LGA with 1% LNG electrode in LGA/$LiCoO_2$ full cells. Fig. 6a presents the voltage profiles of a LGA/$LiCoO_2$ full cell at 0.1, 0.3, 0.5, 1, 3, and 5C. As a comparison, the voltage profiles of a pure graphite and $LiCoO_2$ full cell are shown in Fig. 6b. As it benefited from the N-doped graphene, the specific capacity of our LGA at 0.1, 0.3, 0.5, 1, 3, and 5C is 378, 358, 326, 301, 251, and 159 mA h g^{-1}, respectively, which is superior to that of pure graphite (see Fig. 6b). At a fixed lithiation rate of 0.1C, the cycle stability of pure graphite and the LGA in the full cell is displayed in Fig. 6c. The reversible capacity of the LGA remained at 360 mA h g^{-1} after 100 cycles at 0.1C with a capacity retention of 90%. The cycling stability of the LGA was also superior to that of commercial graphite, which retained a reversible capacity of 320 mA h g^{-1} with a capacity retention of 70% under the same C rate. Additionally, we assembled four LEDs, which were powered by our LGA/$LiCoO_2$ full cells, as shown in Fig. 6d. It is seen clearly from Fig. 6d and S9† that the full cells could light up the blue LEDs. All the bulbs exhibiting favorable brightness confirmed that the LGA could be applied in practical devices instead of the graphite anode.

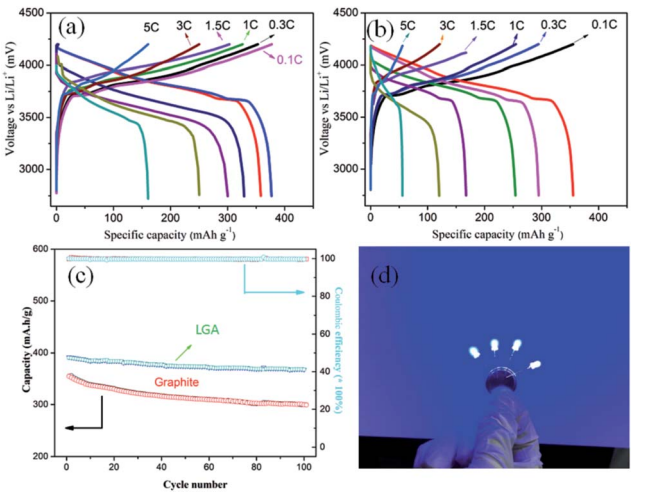

Fig. 6 (a) Voltage profiles of LGA/$LiCoO_2$ full cell. (b) Voltage profiles of pure graphite and $LiCoO_2$ full cell at a rate of 0.1, 0.3, 1, 1.5, 3, and 5C. (c) Cycling performance of LGA/$LiCoO_2$ full cell at 0.1C. (d) Digital photograph of LED powered by LGA/$LiCoO_2$ full cell.

In this report, the performance of LGA electrodes has been shown to greatly improve by the incorporation of only low weight percentages of graphene, owing to the following reasons. First, a very low weight percentage of graphene can fully wrap the graphite particles and form conductive networks (see Fig. S10†). Conversely, excessive graphene can cause the overstacking and agglomeration of graphene, adversely affecting the composite properties. Second, the use of large-size graphene (>10 μm)-coated graphite is key to improving the capacity and rate performance of the composite (see Fig. S11†). We used thermal reduced graphene coated graphite anodes, whose capacity does not exceed the theoretical capacity of graphite (see Fig. S12†). Moreover, Li atoms can be intercalated into the graphene layers, with one Li atom attached to one aromatic ring of the graphene layers to form LiC_6. It was reported that the N-doping of graphene could boost the Li/C ratio[41] and double the reversible discharge capacity of the N-doped graphene compared to pristine graphene,[42] consistent with the results obtained in this work. In addition, LNG can lower the diffusion barriers at both the sides and the center, thus enhancing Li^+ ion mobility. Meanwhile, the warped LNG can enhance the conductivity of the LGA composites and shorten the diffusion paths of the Li^+ ions. In summary, the LNG-coated layers with outstanding conductivity and high Li-storage capacity have not only improved the rate performance of the graphite particles but also promoted synergistic effects between LNG and graphite particles. In the same way, NG has been used to wrap silicon anodes, which greatly improved the capacity and stability of the composite anodes (Fig. S13 and S14†), indicating that this method can be applied to other electrode materials.

Conclusions

A new type of graphite-like carbonaceous anode comprising graphite particles wrapped by large-size LNG platelets was successfully synthesized. The LGA composites containing 1, 3, and 5 wt% of graphene achieved reversible capacities of about 390, 397, and 408 mA h g^{-1}, respectively. The large-size N-doping graphene substantially improved the rate performance of the LGA composite anodes of LIBs, and the convincing full cell properties indicate that the LGA could be a promising anode for high-performance LIBs for a wide range of applications. The new method was also used to wrap other anode materials (*e.g.*, Si) with large-size N-doping graphene. It is anticipated that the method developed for the preparation and incorporation of large-size N-doping graphene into other electrode matrices will stimulate further development of a new class

of electrode materials with enhanced properties and advanced industrial applications.

Acknowledgements

The authors would like to acknowledge support from the National Natural Science Foundation of China (Grant No. 51307046), Natural Science Foundation of Heilongjiang Province of China (Grant No. E2016062), the China Postdoctoral Science Foundation (General Financial Grant No. 2014M561345), the Heilongjiang Postdoctoral Science Foundation (LBH-Z14105), the Scientific Research Foundation for the Returned Overseas Chinese Scholars of the State Education Ministry (No. 20151098), the University Nursing Program for Young Scholars with Creative Talents in Heilongjiang province (No. 2015082), and the Open Project Program of the Key Laboratory for Photonic and Electric Band Gap Materials of the Ministry of Education of Harbin Normal University (No. PEBM201405), The Research Foundation for the Returned Overseas Chinese excellent Scholars of Heilongjiang Province (No. 2015424).

Notes and references

1 M. Armand and J. M. Tarascon, *Nature*, 2008, **451**, 652–657.
2 B. Dunn, H. Kamath and J. M. Tarascon, *Science*, 2011, **334**, 928–935.
3 D. Aurbach, B. Markovsky, I. Weissman, E. Levi and Y. Ein-Eli, *Electrochim. Acta*, 1999, **45**, 67–86.
4 J. Ji, H. Ji, L. L. Zhang, X. Zhao, X. Bai, X. Fan, F. Zhang and R. S. Ruoff, *Adv. Mater.*, 2013, **25**, 4673–4677.
5 J. K. Lee, K. B. Smith, C. M. Hayner and H. H. Kung, *Chem. Commun.*, 2010, **46**, 2025.
6 B. Wang, X. Li, B. Luo, Y. Jia and L. Zhi, *Nanoscale*, 2013, **5**, 1470.
7 M. Zhou, T. Cai, F. Pu, H. Chen, Z. Wang, H. Zhang and S. Guan, *ACS Appl. Mater. Interfaces*, 2013, **5**, 3449–3455.
8 J. Luo, X. Zhao, J. Wu, H. D. Jang, H. H. Kung and J. Huang, *J. Phys. Chem. Lett.*, 2012, **3**, 1824–1829.
9 X. X. Liu, D. L. Chao, Q. Zhang, H. Liu, H. L. Hu, J. P. Zhao, Y. Li, Y. Z. Huang, J. Y. Lin and Z. X. Shen, *Sci. Rep.*, 2015, **5**, 15665.
10 M. H. Park, K. Kim, J. Kim and J. Cho, *Adv. Mater.*, 2010, **22**, 415–418.
11 B. Luo, B. Wang, M. H. Liang, J. Ning, X. L. Li and L. J. Zhi, *Adv. Mater.*, 2012, **24**, 1405–1409.
12 B. Luo, B. Wang, X. L. Li, Y. Y. Jia, M. H. Liang and L. J. Zhi, *Adv. Mater.*, 2012, **24**, 5525.
13 K. Evanoff, J. Khan, A. A. Balandin, A. Magasinski, W. J. Ready, T. F. Fuller and G. Yushin, *Adv. Mater.*, 2012, **24**, 533–537.
14 S. W. Lee, N. Yabuuchi, B. M. Gallant, S. Chen, B. S. Kim, P. T. Hammond and Y. S. Horn, *Nat. Nanotechnol.*, 2010, **5**, 531–537.
15 M. Inoue, Y. Tsuzuki, Y. Iizuka and M. Shimada, *J. Electrochem. Soc.*, 1987, **134**, 756–757.
16 M. Nawa, T. Nogami and H. Mikawa, *J. Electrochem. Soc.*, 1984, **131**, 1457–1459.
17 J. Wang, J. L. Liu, Y. G. Wang, C. X. Wang and Y. Y. Xia, *Electrochim. Acta*, 2012, **74**, 1–7.
18 Z. H. Chen, Q. Z. Wang and K. Amine, *Electrochim. Acta*, 2006, **51**, 3890–3894.
19 K. S. Novoselov, A. K. Geim, S. V. Morozov, D. Jiang, M. I. Katsnelson, I. V. Grigorieva, S. V. Dubonos and A. A. Firsov, *Nature*, 2005, **438**, 197–200.
20 E. Samuel Reich, *Nature*, 2013, **497**, 548.
21 X. X. Liu, D. L. Chao, Y. Li, J. Hao, X. S. Liu, J. P. Zhao, J. Y. Lin, H. J. Fan and Z. X. Shen, *Nano Energy*, 2015, **17**, 43–51.
22 X. Y. Wang, L. Fan, D. C. Gong, J. Zhu, Q. F. Zhang and B. G. Lu, *Adv. Funct. Mater.*, 2016, **26**, 1104–1111.
23 E. Yoo, J. Kim, E. Hosono, H. Zhou, T. Kudo and I. Honma, *Nano Lett.*, 2008, **8**, 2277–2282.
24 G. X. Wang, X. P. Shen, J. Yao and J. Park, *Carbon*, 2009, **47**, 2049–2053.
25 D. Chao, P. Liang, Z. Chen, L. Bai, H. Shen, X. Liu, X. Xia, Y. Zhao, S. V. Savilov, J. Lin and Z. X. Shen, *ACS Nano*, 2016, DOI: 10.1021/acsnano.6b05566.
26 D. Chao, C. Zhu, P. Yang, X. Xia, J. Liu, J. Wang, X. Fan, S. V. Savilov, J. Lin, H. J. Fan and Z. X. Shen, *Nat. Commun.*, 2016, **7**, 12122.
27 C. Y. Wang, D. Li, C. O. Too and G. G. Wallace, *Chem. Mater.*, 2009, **21**, 2604–2606.
28 W. S. Hummers and R. E. Offeman, *J. Am. Chem. Soc.*, 1958, **80**, 1339.
29 X. Liu, D. Zhan, D. Chao, B. Cao, J. Yin, J. Zhao, Y. Li, J. Lin and Z. Shen, *J. Mater. Chem. A*, 2014, **2**, 12166.
30 X. S. Zhou, L. J. Wan and Y. G. Guo, *Adv. Mater.*, 2013, **25**, 2152–2157.
31 G. Q. Wang, W. Xing and S. P. Zhuo, *Electrochim. Acta*, 2013, **92**, 269–275.
32 X. R. Wang, X. L. Li, L. Zhang, Y. Yoon, P. K. Weber, H. L. Wang, J. Guo and H. J. Dai, *Science*, 2009, **324**, 768–771.
33 S. Komaba, M. Watanabe, H. Groult and N. Kumagai, *Carbon*, 2008, **46**, 1184–1193.
34 H. L. Zhang, F. Li, C. Liu and H. M. Cheng, *J. Phys. Chem. C*, 2008, **112**, 7767–7772.
35 S. Komaba, M. Watanabe and H. Groult, *J. Electrochem. Soc.*, 2010, **157**, A1375–A1382.
36 H. Y. Wang, M. Yoshio, T. Abe and Z. Ogumi, *J. Electrochem. Soc.*, 2002, **149**, A499–A503.
37 F. Nobili, S. Dsoke, M. Mancini and R. Marassi, *Fuel Cells*, 2009, **9**, 264–268.
38 M. Yoshio, H. Y. Wang, K. Fukuda, Y. Hara and Y. Adachi, *J. Electrochem. Soc.*, 2000, **147**, 1245–1250.
39 M. Yoshio, H. Y. Wang, K. Fukuda, T. Umeno, T. Abe and Z. Ogumi, *J. Mater. Chem.*, 2004, **14**, 1754–1758.
40 L. H. Hu, F. Y. Wu, C. T. Lin, A. N. Khlobystov and L. J. Li, *Nat. Commun.*, 2013, **4**, 1687.
41 X. K. Kong and Q. W. Chen, *Phys. Chem. Chem. Phys.*, 2013, **15**, 12982–12987.
42 A. L. M. Reddy, A. Srivastava, S. R. Gowda, H. Gullapalli, M. Dubey and P. M. Ajayan, *ACS Nano*, 2010, **4**, 6337–6342.